Velocity and density scaling at the outlet of a silo and its role in the expression of the mass flow rate

D. Maza, A. Janda, S. M. Rubio-Largo, I. Zuriguel, and R. C. Hidalgo

Citation: AIP Conf. Proc. **1542**, 674 (2013); doi: 10.1063/1.4812021

View online: http://dx.doi.org/10.1063/1.4812021

View Table of Contents: http://proceedings.aip.org/dbt/dbt.jsp?KEY=APCPCS&Volume=1542&Issue=1

Published by the AIP Publishing LLC.

Velocity and Density Scaling at the Outlet of A Silo and Its Role in the Expression of the Mass Flow Rate

D. Maza, A. Janda, S.M. Rubio-Largo, I. Zuriguel and R.C. Hidalgo

Departamento de Física y Matemática Aplicada, Facultad de Ciencias, Universidad de Navarra, Navarra, 31080, Spain

Abstract. The role of density and velocity profiles in the flow of particles through apertures has been recently put on evidence in a two-dimensional experiment (Phys. Rev. Lett. 108, 248001). For the whole range of apertures studied, both velocity and density profiles are selfsimilar and the obtained scaling functions allow to derive the relevant scales of the problem. Indeed, by means of the functionality obtained for these profiles, an exact expression for the mass flow rate was proposed. Such expression showed a perfect agreement with the experiential data. In this work, we generalize this study to the three dimensional case. We perform numerical simulations of a 3D silo in which the velocity and volume fraction profiles are determined. Both profiles shows that the scaling obtained for 2D can be generalized to the 3D case. Finally, the scaling of the mass flow rate with the outlet radius is discussed.

Keywords: Silo, Flow rate
PACS: 83.10, 83.10.Rs

INTRODUCTION

The flow of particles through bottlenecks is an ubiquitous situation in industry. Despite this fact, an established theoretical description of the particle mass flow rate through an orifice, is still lacking. Back in the the sixties, a phenomenological relation was introduced by Berveloo [1] to quantify the flow rate coming out from and orifice. In fact, Beverloo's expression is massively used and it gives good predictions for the flow rate in certain ranges of outlet apertures. However, its derivation takes into account strong empirical arguments such as the existence of an effective outpouring diameter or a volume fraction at the exit that equals the bulk value.

Since the introduction of Berberloo's law, a large number of minor modifications have been proposed by other authors [2]. Recently, Mancok *et. al.* [3] proposed an alternative expression covering a wider range of outlet sizes, starting from the diameter of a grain. In this expression – also empirically motivated – k factor is fixed to one and a multiplicative exponential factor is considered. The authors speculated that this factor is related to a volume fraction reduction near to the outlet. Importantly, the outcomes extracted from former works are mainly sustained in dimensional analysis and not in rigorous theoretical calculations at the silo outlet. Certainty this topic has been profusely discussed by many authors [4], but without any conclusive result about the origin of the collective behavior shown by the material. One of the main reasons for that is the intrinsic difficulty that the prediction of the velocity profiles implies.

Additionally, the stress propagation inside a silo is also an open question and the role of the volume fraction and its relationship with the velocity profile remains undetermined. Those aspects are particularly important in the region of the outlet, where a continuity argument should be applied to calculate the mass flow rate.

Very recently, this framework has been systematically studied by Janda *et. al.* [5]. In that work, they experimentally showed that the profiles of the vertical velocity, $\mathbf{v}$, and volume fraction, ϕ, just at the exit of a flowing silo display a well defined functionality. The analysis was performed in a quasi-bidimensional silo where volume fraction and velocity field are optically accessible. Under this condition, the authors demonstrated that the profiles of both magnitudes as a function of the outlet radius R can be expressed as:

$$\mathbf{v}(r) = \sqrt{2gR}\sqrt{1-(r/R)^2} \tag{1}$$

$$\phi(r) = \phi_\infty[1-\alpha e^{-R/\beta}]\left[1-(r/R)^2\right]^{1/\nu} \tag{2}$$

where g is the gravity acceleration and ϕ_∞, α, β and ν are fitting parameters with certain physical meaning. Using both expressions the mass flow rate on the exit line results in:

$$W = C''\sqrt{g}\phi_\infty\left[1-\alpha e^{-R/\beta}\right]R^{3/2} \tag{3}$$

where C" is a constant, which only depends on the exponent ν in Eq. 2.

In the present work, we numerically analyze the same situation but for circular orifices in the base of a flat bottomed 3D silo. We demonstrate that both profiles display the same functionality and, as a consequence, Eq. 3 can be generalized to the three dimensional case.

Powders and Grains 2013
AIP Conf. Proc. 1542, 674-677 (2013); doi: 10.1063/1.4812021

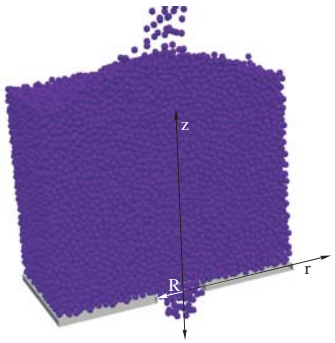

FIGURE 1. Vertical section of the numerical silo. z=0, r=0 corresponds to the center of the orifice of radius R.

NUMERICAL ANALYSIS

We have performed Discrete Element Modeling (DEM) of a system of monodisperse spheres with radio $r_p = 1/64\ m$. To mimic the real experimental scenario, we generate a granular column from a granular gas of 131072 particles. Once the particles are located at random positions, within a cylindrical container with flat bottom, they settle under the effect of gravity. The particles are allowed to leave the system through a circular outlet, which is located at the bottom of the column. The cylindrical container has a radius $R_c = 32 \times r_p$ and its walls are considered to have similar mechanical properties than the particles. Our procedure allow us to continually control the granular flow through the outlet even so all micro-mechanical properties of the silo. In the present work, we examine the behavior of the particle flow in the outlet by studying the velocity and volume fraction profiles. Thus, the radius of the outlet has been varied from $R = 7 \times r_p$ to $R = 13 \times r_p$.

In the simulation, each particle i $(i = 1...N)$ has three translational degrees of freedom and a quaternion formalism has been implemented for describing the $3D$ angular rotations. The interaction between particle i and particle j, $\vec{F}_{ij}$, is decomposed as,

$$\vec{F}_{ij} = F_{ij}^N \cdot \hat{\vec{n}} + F_{ij}^T \cdot \hat{\vec{t}}, \tag{4}$$

where F_{ij}^N is the component on the normal direction $\hat{\vec{n}}$ to the contact plane. In the same way, F_{ij}^T is the component acting on the tangential direction $\hat{\vec{t}}$. In our approach, the normal interaction F_{ij}^N, is defined by a linear contact. Moreover, to introduce dissipation, a velocity dependent viscous damping is assumed. Hence, the total normal force reads as

$$F_{ij}^N = -k^N \delta - \gamma^N v_{rel}^N, \tag{5}$$

where k^N is the spring constant on the normal direction, γ^N is the damping coefficient in the normal direction and v_{rel}^N is the normal relative velocity between i and j. Moreover, the tangential force F_{ij}^T also includes an elastic term and a tangential frictional term accounting for static friction between the grains. This takes into account the Coulomb friction constrain as

$$F_{ij}^T = \min\{-k^T \xi - \gamma^T m_r \cdot |v_{rel}^T|, \mu F_{ij}^N\}, \tag{6}$$

where γ^T is the damping coefficient in tangential direction, v_{rel}^T is the tangential component of the relative contact velocity of the overlapping pair. ξ represents the elastic elongation of an imaginary spring with spring constant k^T at the contact [6], which increases as $d\xi(t)/dt = v_{rel}^T$ as long as there is an overlap between the interacting particles [6, 7]. μ is the friction coefficient of the particles. The kinematic tangential relative displacement $\xi(t)$, is updated using a Euler's algorithm. The equations of motion are integrated using a Fincham's leap-frog algorithm (rotational) [9] and a Verlet Velocity algorithm (translational) [8].

We have modeled hard particles introducing values for normal and tangential elastic constants, $\frac{k_t}{k_n} = 2/7$ with $k_n = 10^8 N/m$. The ratio between normal and tangential damping coefficients is taken as $\frac{\gamma_n}{\gamma_t} = 3$, the density of the particle $\rho = 7520\ kg/m^3$, while gravity is set to $g = 10\ m/s^2$. These parameters have been chosen to model the steel beads used in the experiments. The time step used for these parameters was set as$\Delta t = 10^{-6} s$. In all the examples reported here, we have used this set of parameters and only the diameter of the outlet has been changed. Finally, it is important to remark that we have developed a hybrid (CPU-GPU) DEM algorithm, which has allowed us to simulate 131072 particles, in reasonable computing times. Complementary, we have executed similar calculations using the Open Source code LIGGGHTS, using 50000 particles and similar results came out.

VOLUME FRACTION AND VELOCITY PROFILES

Velocity and volume fraction profiles have been determined for four distinct outlet radius R. In order to avoid transitory regime, the particles are allowed to flow a few seconds; later on, the profiles have been examined. The mean vertical velocity as a function of the radial coordinate $\mathbf{v}(r)$, was calculated accounting for all the particles that cross a plane defined by the bottom wall. At same location, the volume fraction was numerically determined. The procedure was the following: we have numerically calculated the overlap volume between each particle and

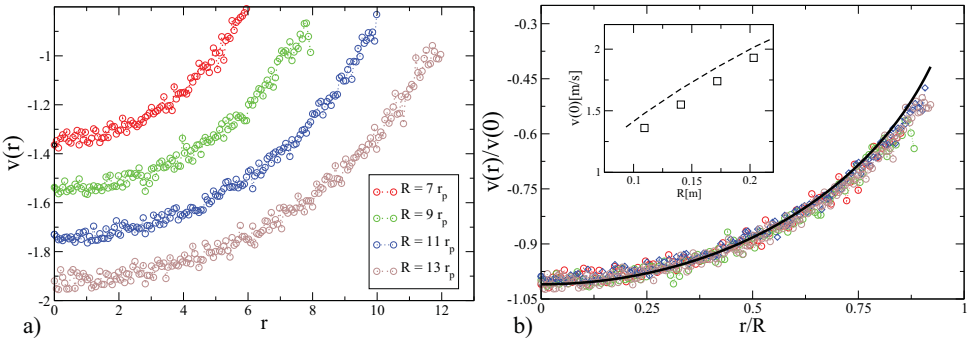

FIGURE 2. a) Velocity profiles (averaged in the azimuthal direction) obtained for different outlet radius. (b) The same data collapsed by the scale factors introduced in Eq. 1. The continuous line is the correspond to $-\sqrt{1-(r/R)^2}$. Inset: Velocity at the center of the orifice, $\mathbf{v}(0)$, as a function of the outlet radius R. The dashed line display $\sqrt{2gR}$.

a rectangular prism of height $h = 2 \times r_p$. The base of the prism is located at the outlet of the silo and it has been discretized with accuracy $\Delta x = \Delta y = \frac{1}{26} r_p$. In each case, at least twenty configurations were averaged and the system was sampled every 0.1 seconds. Finally, we have taken into account the cylindrical symmetry, reporting the radial dependence of the mean volume fraction $\phi(r)$.

Figure 2.a shows the profiles obtained for the outlets analyzed. Clearly, all the profiles display the same functionality. Similar to Ref.[5], all the data points can be collapsed into a single curve by normalizing the radial coordinate with the outlet radius and the velocity with the velocity at the centre of the orifice, $\mathbf{v}(0)$. Remarkably, for each radius, the maximum velocity differs less than 10% than the velocity predicted by the scale factor Eq. 1 (see inset Fig. 2.b). Moreover, Fig. 2.b. illustrates that the scaling function $\sqrt{1-(\frac{r}{R})^2}$ reproduces very well the collapsed data. The scale factor $\sqrt{2gR}$ can be justified assuming the existence of a region, above the orifice, below which the grains fall freely under the gravity. This hypothetical region scales with the outlet aperture R and it was early introduced by Hagen [10] and lately developed by Brown & Richards [11] under the name of "free fall arch". Following the original idea of Hagen, the scaled expression (Eq. 1)is compatible with the existence of a hypothetical *parabolic* dome, beyond which the beads fall only under the gravity action (see Ref. [5] for a detailed explanation of this idea). Finally, averaging Eq. 1 along the outlet, the scaling for the average velocity with $R^{1/2}$ is obtained. It is important to remark that this factor is usually introduced in the literature without a formal explanation.

The volume fraction profiles $\phi(r)$ along the exit have also been examined (Fig. 3.a). In this case, two salient features must be remarked: (a) the packing decreases close to the edges with a well defined functionality and, (b) the mean value for the volume fraction is clearly lower than the bulk density, $\phi_{bulk} = 0.64$. These features were reported by using an elegant experimental setup at the early seventies by Van Zuilichem *et. al.* [12] but this work has been scarcely considered until now. In addition, it is obvious that $\phi(r)$ is not null even near the limit of the orifice. As in the case of the velocity, the volume fraction profiles are self-similar and can be rescaled by the volume fraction at the center of the outlet, $\phi(0)$. The collapsed data are plotted in Fig. 3.b where the agreement with $\frac{\phi(r)}{\phi(0)} = \sqrt[4]{1-(r/R)^2}$ is noted. However, the scaled expression fails for points very close to the border of the orifice, which is partially related with the finite size of the bottom wall. Nevertheless, the error introduced by this part of the profile on the calculus of the averaged volume fraction is lower than 1%. Let us now focus on the dependency of $\phi(0)$ on R. Fig. 3.a shows that the maximum value of the volume fraction depends on the radius of the orifice. Further calculations are needed to confirm the volume fraction asymptotic growth, which has been predicted for the two-dimensional case (see exponential prefactor of Eq. 2). However, the tendency of these values versus R is clearly nonlinear (as reported in [12]) and, of course, should converge asymptotically to a finite value.

DISCUSSION

Our numerical results show the self-similar shape of the velocity and density profiles in 3D silos. Their corresponding scale functions do not include an explicit functionality with r implying relevant consequences in the calculus of the mass flow rate. Indeed, Eulerian description of the mass conservation law implies that the formal expression for the *mean* mass flow rate can be calculated from the spatial integral of $< \phi(r)\mathbf{v}(r) >$, where the brackets indicate a volume-time averaging process [13].

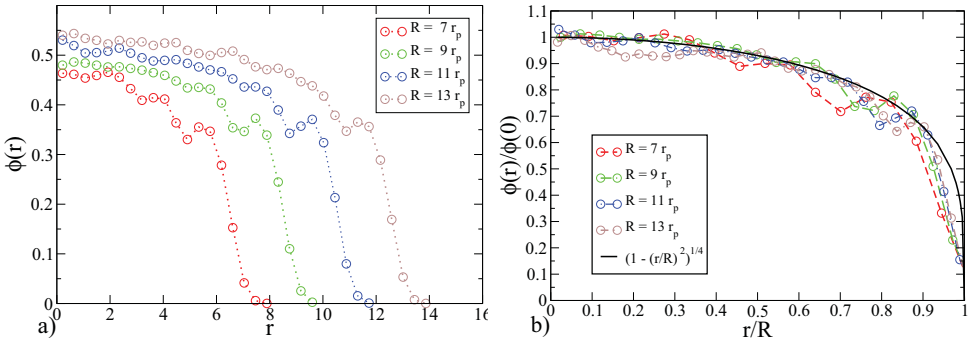

FIGURE 3. (a) Packing fraction profiles for different outlet sizes. (b) Collapsed volume fraction profiles corresponding to the data displayed in (a). The continuous line is the scaling function introduced in the text.

Although deep inside of the silo both profiles are strongly coupled, just in the region of the orifice, is reasonable to assume that both magnitudes describe uncorrelated fluctuation at temporal scales larger than the time required for a particle to freely fall its own diameter. Hence, the mean mass flow rate can be calculated as: $W =< \phi(r) >< \mathbf{v}(r) > A$, where A is the area of the orifice. As the scale function used to collapse both profiles does not depend explicitly on the variable r, both averages will depend on an expressions like $[1-(\frac{r}{R})^2]^{\frac{1}{\nu}}$. There, we have used $\nu = 4$ ($\nu = 2$) to collapse the packing (velocity) profile (Figs. 2.b and 3.b). Independently of the exact value of these exponents, the spatial integral of this kind of function gives a multiplicative constant times the radius of the orifice. Therefore, the final expression for W will include factors related with the profile shapes times $R^{5/2}$. This result is in complete agreement with the exact expression obtained for the two dimensional case (Eq. 3) putting on evidence the importance of considering the spatial dependence of the velocity and volume fraction to calculate the mass flow rate. Moreover, due to the revolution symmetry of both profiles the extension to the 3D case is trivial and the predicted flow fits very well the experimental data [3]. Importantly, the calculus does not include any consideration about an *effective* exit size or *hydraulic diameter*, represented by the k parameter [1]. Instead, the details of the flow for any orifice radius are described by the volume fraction dependence [5]. Finally, let us remark that the self-similarity of both profiles predicts the validity of the flow expression even for large outlet apertures, where intuitively we tend to assume a plug profile for the velocity field.

ACKNOWLEDGMENTS

This work has been supported by Projects FIS2011-26675 (Spanish Government) and PIUNA (Universidad de Navarra). S.M. Rubio-Largo thanks Asociación de Amigos de la Universidad de Navarra for a scholarship.

.

REFERENCES

1. W.A. Beverloo, H.A. Leniger, J. J. Van de Velde. *Chem. Eng. Sci.* **15**, 260-296 (1961).
2. R.M. Nedderman. "Chapter 10: The prediction of the mass flow rate", *Static and Kinematic of Granulars Materials.* Cambridge University Press, Cambridge, 1992, pp. 292-326.
3. C. Mankoc, A. Janda, R. Arévalo, J.M. Pastor, I. Zuriguel, A. Garcimartín, D. Maza. *Granular Matter* **9**, 407-414 (2007).
4. R.M. Nedderman. "Chapter 8: Velocity distribution", *Static and Kinematic of Granulars Materials.* Cambridge University Press, Cambridge 1992, pp. 243-372.
5. A. Janda, I. Zuriguel & D. Maza. *Phys. Rev. Lett.* **108**, 248001–5 (2012).
6. P. Cundall and O. Strack, *Geotechnique* **29**, 47–65 (1979)
7. G. Duvaut and J.-L. Lions, *Les Inéquations en Mécanique et en Physique*. Dunod, Paris, 1972.
8. L. Verlet, *Phys. Rev.*, **165**, 201-214 (1968)
9. D. Fincham, "Leapfrog rotational algorithms," *Molecular Simulation*, **8** 165-178 (1992)
10. English version of this paper can be found in: Granular Matter **9**, DOI 10.1007/s10035-006-0027-x, (2006).
11. Brown, R.L., Richards, J.C.: *Principles of Powder Mechanics.* and references therein. Pergamon Press, Oxford, 1970.
12. Van Zuilichem, D.J. Van Egmond, N.D. De Swart , J.G. Powder Tech. **10**, 161-169 (1974).
13. Liang-Shih Fan and Chao Zhu. "Chapter 5: Basic Equations", *Principles of Gas-Solid Flows.* Cambridge Series in Chemica Engineering, Cambridge Press. Cambridge, 1997, pp. 164-242.